The Enigma of the Liganded Hemoglobin End State: A Novel Quaternary Structure of Human Carbonmonoxy Hemoglobin[†,‡]

M. K. Safo* and D. J. Abraham

School of Pharmacy, Department of Medicinal Chemistry, and Institute for Structural Biology and Drug Discovery, Virginia Commonwealth University, Richmond, Virginia 23219

Received March 3, 2005; Revised Manuscript Received April 15, 2005

ABSTRACT: The liganded hemoglobin (Hb) high-salt crystallization condition described by Max Perutz has generated three different crystals of human adult carbonmonoxy hemoglobin (COHbA). The first crystal is isomorphous with the "classical" liganded or R Hb structure. The second crystal reveals a new liganded Hb quaternary structure, RR2, that assumes an intermediate conformation between the R form and another liganded Hb quaternary structure, R2, which was discovered more than a decade ago. Like the R2 structure, the diagnostic R state hydrogen bond between β2His97 and α1Thr38 is missing in the RR2 structure. The third crystal adopts a novel liganded Hb conformation, which we have termed R3, and it shows substantial quaternary structural differences from the R, RR2, and R2 structures. The quaternary structure differences between T and R3 are as large as those between T and R2; however, the T → R3 and T → R2 transitions are in different directions as defined by rigid-body screw rotation. Moreover, R3 represents an end state. Compared to all known liganded Hb structures, R3 shows remarkably reduced strain at the α-heme, reduced steric contact between the β-heme ligand and the distal residues, smaller α- and β-clefts, and reduced $\alpha1-\alpha2$ and $\beta1-\beta2$ iron−iron distances. Together, these unique structural features in R3 should make it the most relaxed and/or greatly enhance its affinity for oxygen compared to the other liganded Hbs. The current Hb structure−function relationships that are now based on T → R, T → R → R2, or T → R2 → R transitions may have to be reexamined to take into account the RR2 and R3 liganded structures.

Perutz (*1*, *2*) and Baldwin and Chothia (*3*) analyzed at atomic resolution the structures of the T (tense or unliganded) and R (relaxed or liganded) forms of Hb[1] embodied in the two-state MWC model (*4*), which assumes that the T and R states are in equilibrium with each other and allosterically switch without intermediate states. The T state has a low affinity for ligands, while the R state has a high affinity for ligands. The two-state MWC model has been challenged by the discovery of a new ligand-bound Hb structure known as R2 (*5*) or Y (*6*, *7*). The R2 structure has been proposed as an intermediate between the T and R structures (*5*−*7*). Further analysis has shown that R2 is not an intermediate, but rather another liganded end state structure (*8*, *9*). Srinivasan and Rose (*10*) and Schumacher et al. (*11*) have further suggested that R2 may be the physiologically relevant liganded end state structure and that R is an intermediate trapped between the R2 and T structures by the high-salt crystallization conditions. In contrast, the R2 structure formation is believed to be favored by low-salt conditions that mimic in vivo conditions (*5*−*7*, *10*). In the past decade, more studies have also revealed the existence of other liganded Hb structures, including a human embryonic Gower II ($\alpha2\epsilon2$) carbonmonoxy Hb (*12*), bovine carbonmonoxy Hb (*13*, *14*), and cross-linked forms of human carbonmonoxy Hb (*11*), all with quaternary structures that are positioned between the R and R2 structures. In contrast to the different liganded quaternary structures, only one Tense or unliganded structure has been reported when crystallized from high salt (*15*) or from low salt (*16*).

This paper describes two new human adult carbonmonoxy hemoglobin structures in the relaxed conformation. The crystals were discovered inadvertently during liganded Hb crystallization experiments. One of the crystal structures is termed RR2, because it assumes a conformation that is almost equilaterally between those of the R and R2 structures. The RR2 structure is similar in conformation to those reported for Gower II COHb (PDB entry 1AJ9), bovine COHb (PDB entries 1FSX, 1G08, and 1G09), and cross-linked forms of COHbA (PDB entries 1HAB and 1HAC). The T → RR2 and T → R2 shifts are similar and in the same direction as defined by rigid-body screw rotation (*3*, *13*, *17*); however, the R2 shift is more extensive than that of RR2. The other crystal structure, termed R3, is a novel liganded Hb structure that appears to be an end state. In fact, the T → R3 shift is comparable in magnitude to the corresponding T → R2 shift;

[†] We gratefully acknowledge research support from the National Institutes of Health to M.K.S. (Grant HL04367) and to D.J.A. (Grant HL32793).

[‡] The atomic coordinates and structure factors have been deposited in the RCSB Protein Data Bank as entries 1MKO and 1YZI for the RR2 and R3 Hb structures, respectively.

* To whom correspondence should be addressed: Institute for Structural Biology and Drug Discovery, 800 E. Leigh St., Suite 212, Richmond, VA 23219. Phone: (804) 828-7291. Fax: (804) 827-3664. E-mail: msafo@mail2.vcu.edu.

[1] Abbreviations: Hb, hemoglobin; HbA, normal human adult hemoglobin; COHb, carbonmonoxy hemoglobin; 2,3-DPG, 2,3-diphosphoglycerate.

10.1021/bi050412q CCC: $30.25
Published on Web 05/21/2005

however, they differ in direction. The results from these studies raise some basic questions: Are all these liganded Hb structures, including R, RR2, R2, and R3, physiologically relevant, and if so, which represents the end state? What is the allosteric pathway between the different Hb states? The data presented here provide some significant insight into the allosteric mechanism, and may help to clarify some Hb functional observations.

EXPERIMENTAL PROCEDURES

Materials and Methods. Procedures for crystallizing Hb in both RR2 and R3 states have previously been described (*18*) and are very similar to the method used by Perutz to crystallize R state Hb (*19*). Briefly, a HbA solution was evacuated for ~10 min, and the resulting deoxygenated solution was further reduced by addition of a small pellet of $Na_2S_2O_4$. The deoxygenated HbA solution was then saturated with CO to generate the CO-bound HbA form. Crystallization was carried out with a solution of 30−40 mg/mL protein and 3.2−3.4 M sodium/potassium phosphate at various pHs (including 7.6, 7.1, 6.7, 6.4, 5.9, 5.7, 5.4, and 5.0) using 7 mL vacutainer tubes. One to two drops of toluene was added to the COHbA solution in each tube. More CO was bubbled into the tubes, and then the tubes were sealed. Crystals appeared in several of the tubes (see below) containing a final phosphate concentration of 2.25−2.75 M.

X-ray diffraction data sets for the RR2 and R3 crystals obtained at pH 6.7 and 7.1, respectively, were collected at 120 K using a Molecular Structure Corp. (MSC, The Woodlands, TX) X-Stream Cryogenic Cooler System, an R-Axis II image plate detector equipped with OSMIC mirrors, and a Rigaku RU-200 generator operating at 50 kV and 100 mA. Prior to use in diffraction, the crystals were first washed in a cryoprotectant solution containing 50 μL of mother liquor and 10−15 μL of glycerol. The data sets were processed with MSC BIOTEX. The X-ray data for all complexes are summarized in Table 1.

The structures of the R3 and RR2 crystals were determined by the molecular replacement methods (*20*). For the R3 crystal, the $\alpha 1\beta 1$ dimer of the R (PDB entry 1HHO) structure was used as the search model. Space group $P4_122$ gave a unique solution of a dimer in the asymmetric unit with a final correlation coefficient of 66.2 and an *R*-factor of 38.8% at 4.0 Å. Refinement of the molecular replacement model using CNS (*21*) resulted in a final crystallographic *R*-factor and R_{free} of 20.8 and 25.7%, respectively, at 2.07 Å.

For the RR2 crystal, the R (PDB entry 1HHO) and R2 (PDB entry 1BBB) tetramer structures were independently used as search models. Both models provided solutions at 4.0 Å, with the R2 model exhibited a final higher correlation coefficient and *R*-factor of 54.0 and 40.8%, respectively, suggesting the closeness of the RR2 and R2 structures. Final refinement of the model using CNS (*21*) resulted in an *R*-factor of 20.3% and an R_{free} of 28.2% at 2.18 Å.

Model building and correction were carried out using TOM (*22*). All figures, with the exception of Figure 6, were generated with INSIGHTII (Molecular Simulations, Inc., San Diego, CA) and labeled with SHOWCASE. Figure 6 was generated with ChemDraw. The crystallographic data are summarized in Table 1.

Table 1: Crystal Information, Data Collection, and Refinement Parameters for the R3 and RR2 Structures[a]

	R3	RR2
data collection statistics		
space group	$P4_122$	$P2_12_12_1$
unit cell dimensions (Å)	61.46, 61.46, 174.75	65.53, 154.57, 55.27
no. of molecules/asymmetric unit	1 dimer	1 tetramer
resolution (Å)	2.07 (2.20−2.07)	2.18 (2.28−2.18)
no. of unique reflections	20310 (2522)	27473 (2344)
$I/\sigma I$	13.1 (2.0)	13.2 (3.3)
completeness (%)	95.2 (76.7)	91.0 (63.3)
redundancy	5.6	4.5
R_{merge} (%)[b]	6.7 (25.3)	6.5 (22.8)
structure refinement		
resolution limit (Å)	60−2.07 (2.20−2.07)	60−2.18 (2.32−2.18)
σ cutoff (F)	0.0	1.0
no. of reflections	20310 (2522)	26700 (2993)
completeness	95.2 (76.7)	88.7
R-factor (%)	20.8 (28.6)	20.3 (21.8)
R_{free} (%)[c]	25.7 (29.8)	28.2 (30.4)
rmsd from standard geometry		
bond lengths (Å)	0.018	0.017
bond angles (deg)	2.2	2.2
positional error (Luzzati)		
R-factor	0.25	0.24
R_{free}	0.31	0.35
dihedral angles		
most favored regions	89.2	91.0
additional allowed regions	10.8	9.9
average *B*-factors (Å^2)		
all non-hydrogen atoms	47.6	32.6
protein atoms	47.4	32.5
heme atoms[d]	48.4	25.7
CO atoms[d]	36.6	22.6
water atoms	50.1	36.4
phosphate atoms	−	66.1
toluene atoms	45.6	−

[a] Numbers in parentheses refer to the outermost resolution bin. [b] $R_{merge} = \sum(\langle I\rangle - I)/\sum I$. [c] Five percent of the reflections which were used for the calculation of R_{free} were excluded from the refinement. [d] Note that the average *B*-factor of β-heme is 56.4 Å^2, compared with a value of 40.3 Å^2 for the α-heme (see the text).

RESULTS AND DISCUSSIONS

Crystallization Studies. Our initial purpose was to obtain COHbA crystals in the R conformation using high-salt conditions as described by Perutz (*19*). Surprisingly, we obtained rectangular needle crystals in space group $P4_122$, and the following approximate unit cell constants: $a = 62$ Å, $b = 62$ Å, and $c = 176$ Å. This is in contrast to the usual octahedral R crystals, which are known to crystallize under this condition in space group $P4_12_12$. The ensuing crystal structure is termed R3.

Further crystallization experiments resulted in another crystal type, termed RR2. The RR2 crystals are also needlelike but grow thinner and longer than those of the R3 crystals, and belong to orthorhombic space group $P2_12_12_1$, with the following approximate unit cell constants: $a = 65$ Å, $b = 154$ Å, and $c = 55$ Å. In view of the results described above, several crystallization experiments using high-salt conditions and various pHs (5.0−7.6) were conducted to determine the effect of pH on crystal type. At pH 5.0−7.6, the crystals were predominately R and R3 forms that occur sometimes alone, or with each other in varying amounts. However, at the low pHs (5.0 and 5.4), R3 crystals occur in greater frequency than R crystals. Unlike R or R3 crystals, RR2 crystals are obtained occasionally, and only in small

quantities at pH 6.4−7.1. The RR2 crystals mostly occurred in combination with the more abundant R crystals. There seems to be a pH effect on crystal type, but it is very difficult to rationally correlate the relationship between the two since repeat experiments did not give consistent results.

We also point to the fact that on one occasion platelike crystals were obtained. Unfortunately, we were unable to characterize the crystal because of poor diffraction. Most likely, this crystal is structurally different from the R, RR2, or R3 crystals. The R3 and perhaps RR2 crystals may have been those observed and ignored in previous crystallization experiments in our laboratory during the past 14 years which have produced different crystal morphologies, sometimes alone or in the presence of well formed octahedral R crystals. These new crystals for the most part occurred as thin rectangular needles which we never analyzed.

Perutz (*23*) and Green et al. (*24*) previously reported that crystals of horse liganded Hb changed lattice at pH 6.0, with a concomitant decrease of ∼4 Å in the distance between two mercury atoms bound to β1Cys93 and β2Cys93. Recently, two crystal structures of bovine methemoglobin have been published at different pHs, with the structure at pH 5.4 showing a 3.8 Å reduction in the distance between the two sulfur atoms when compared to the structure at pH 7.1. Both structures are in the R conformation; however, the structure at the lower pH has the α-heme group converted to a hemichrome (bishistidine) form (*25*). Interestingly, the R → RR2 and R → R3 shifts have also resulted in decreases of ∼2.2 and ∼4.7 Å in the distance between the β1Cys93 and β2Cys93 sulfur atoms, respectively.

Overall Structure Descriptions of RR2 and R3. The two crystal structures, RR2 and R3, have essentially the same secondary structures as other reported normal human Hbs, consisting of seven helices in the α-subunit and eight in the β-subunit. The final 2.07 Å refined R3 structure contains one α1β1 dimer in the asymmetric unit, two heme groups, two CO ligands, and 136 water molecules. The regions defined by the β-subunit N-terminus (residues 1−3), C-terminus (residues 139−146), E helix−EF corner−F helix−FG corner region (residues 58−103), and the heme are characterized by high *B*-factors: average *B*-factor of 63.3 Å^2, compared with values of 49.3 and 47.6 Å^2 for the analogous α-subunit regions and the whole protein, respectively. The high *B*-factors may be due to lack of crystal packing, as most of these residues are exposed to the bulk solvent. Nonetheless, the electron densities are well defined with the exception of the N-terminal and C-terminal residues of βVal1, βTyr145, and βHis146. Interestingly, these flexible regions form the β-cleft as well as the residues around the β-heme.

Toluene which is routinely used to aid in the crystallization process of liganded Hb binds to the R3 structure at three locations. Two of the toluene molecules are located within the protein in a hydrophobic pocket formed by αTrp14, αVal17, αTyr24, αLue105, αLeu109, αLeu125, αPhe128, αVal10, αVal70, and αLeu66, while the third molecule is located at the surface of the protein in a cleft formed by residues αAsn9, αAla13, αLys16, αLeu109, αLeu103, αGlu116, and αVal121. Two toluene molecules were also found bound to a natural mutant, Hb Bassett in the R conformation (*26*), at the former site described for the R3 structure. This site (in both T and R structures) is also known to bind to antigelling agents, including dichloromethane (*27*), iodobenzene, and *p*-BrBzIOH (*28*). It has been proposed that binding of a compound at this site helps to destabilize the formation of HbS polymer to prevent erythrocyte sickling (*27*, *29*−*31*).

The final 2.18 Å refined model for the RR2 structure contains a single α1β1α2β2 Hb tetramer in the asymmetric unit, four heme groups, four CO ligands, and 326 water molecules. One of the three phosphate ions found in the model is located on the dyad axis at the C-terminal end of the β-subunit (β-cleft), where residues β1His143, β2His143, β1His146, and β2His146 in the 2,3-diphosphoglycerate (2,3-DPG) binding site in T state Hb (*32*, *33*) form an almost perfect tetrahedral hydrogen bond arrangement around the phosphate. Like the R3 structure, the β-subunit N-terminus, C-terminus, and E helix−EF corner−heme−F helix−FG corner region of the RR2 structure also exhibit high *B*-factors; however, the lability is not as pronounced as in the R3 structure. Also, like the R3 structure, these regions are mostly exposed to the bulk solvent.

We have previously published the crystal structure of R COHbA (PDB entry 1LJW) using crystals obtained during the crystallization experiments described above (*34*). This structure is conformationally indistinguishable from other R quaternary structures; however, the α1β2 dimer interface shows significant weakening, as well as T state characteristics (*34*).

Quaternary Structures. The RR2 and R3 structures were compared with the T deoxygenated HbA (PDB entry 2HHB), the R COHbA (PDB entry 1AJ9), and the R2 COHbA (PDB entry 1BBB) structures. Tetramers were generated by application of crystal symmetry for the R and R3 structures, which have only a single α1β1 dimer in the asymmetric unit. Figure 1 shows the α1β2 dimers, as well as the switch and joint interfaces of the five Hb structures, after superposition of the α1β1 dimers (Cα residues) on the B helix−G helix−H helix (BGH) frame (*3*) with the T structure as a reference point. It is apparent that the quaternary structures of all five Hbs are significantly different from each other. Moreover, the switch regions show large differences in residue positioning compared to the joint regions. Baldwin and Chothia (*3*) were the first to characterize the α1β2 (α2β1) dimer interface as consisting of both switch and joint regions. They noted that transition between the T and R quaternary forms resulted in significant changes in the relative positions of the residues in the switch region, while residue positions in the joint region remained relatively unchanged. Analyses of the hydrogen bond contacts between the α1β2 dimer interface of the above structures are given in Table 2. As expected, the T structure hydrogen bond interactions at the switch region are different from those of the liganded structures. Among the liganded structures, there are two distinct differences. First, the R state diagnostic hydrogen bond interaction between α1Thr38 and β2His97 is also observed in the R3 structure but missing in the RR2 and R2 structures. This is due to differences in the position of the β2-subunit relative to the α1-subunit at the switch region (see below). Second, a hydrogen bond interaction between α1Thr41 and β2Arg40 in R, RR2, and R2 structures is significantly lengthened to 4.1 Å in the R3 structure. However, we note that the side chain of β2Arg40 in R3 has oriented to make a hydrogen bond with α1Leu91 at the joint region (Table

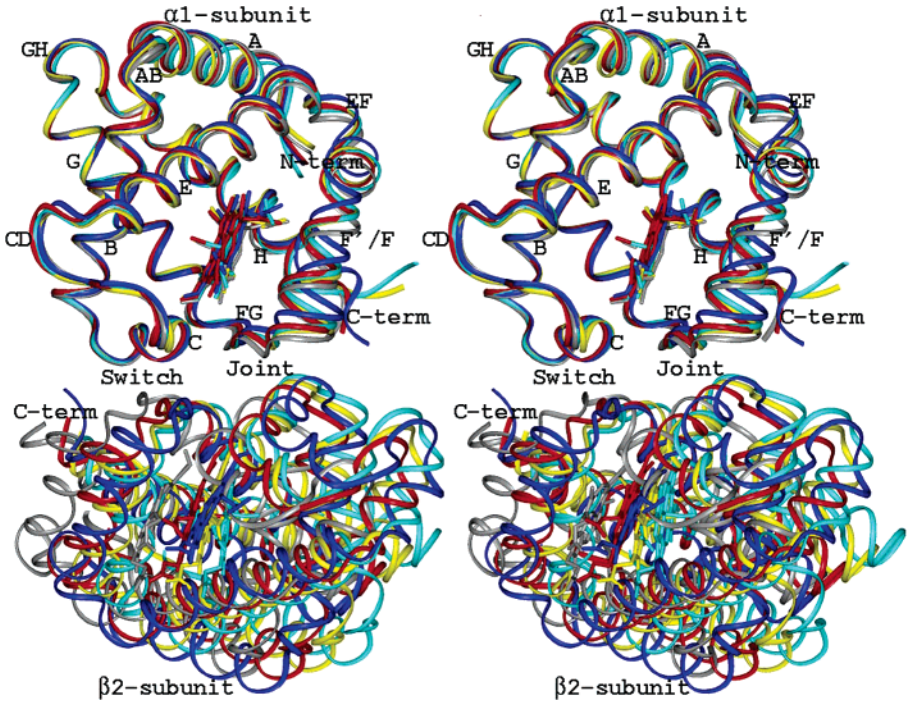

FIGURE 1: Stereofigure of the overlay of the α1β2 dimers showing the N- and C-terminal, joint, and switch regions of T (blue Cα trace), R (red Cα trace), RR2 (yellow Cα trace), R2 (cyan Cα trace), and R3 (gray Cα trace) structures. The structures were superimposed with the α1β1 dimer as described in the text. The nonsuperimposed regions (β2 subunits) show large quaternary structural differences, while the superimposed regions (α1 subunits) as expected show similar structural conformations with only significant tertiary structural differences in the EF corner−F helix−FG corner region as well as the N- and C-termini.

Table 2: Hydrogen Bond Interactions at the α1β2 Dimer Interface of the T, R, RR2, R2, and R3 Hb Structures[a]

contact		T	R	RR2	R2	R3
Switch Region						
α1Thr38 OH	β2His97 O	–	2.4	–	–	2.4
α1Tyr42 OH	β2Asp99 OD1	2.5	–	–	–	–
α1Thr41 O	β2Arg40 NH2	–	2.9	3.1	3.5	–
α1Asp94 OD2	β2Asn102 ND2	–	3.2	2.8	2.7	2.8
α1Asn97 ND2	β2Asp99 OD1	2.8	–	–	–	–
Joint Region						
α1Leu91 O	β2Arg40 NE	2.8	–	–	–	2.8
α1Arg92 NH2	β2Gln39 OE1	–	–	2.9	–	–
α1Arg92 NH2	β2Glu43 OE1	–	–	–	3.1	–
α1Arg92 O	β2Arg40 NE	3.3	–	–	–	–
α1Asp94 OD1	β2Trp37 NE1	3.0	3.3	3.6	3.6	3.5

[a] In the structures with a tetramer in the asymmetric unit, the contact distances shown are those between the α1β2 interface. Similar contact distances are also observed at the α2β1 contact region.

2). The different interactions may not be unique since the side chain of β2Arg40 which is located between residues α1Thr41 and α1Leu91 in all the liganded structures is capable of reorienting to make contact with either α1Thr41 (switch interface) or α1Leu91 (joint interface). There are also significant differences in the hydrogen bonds observed at the joint regions. Among the liganded structures, a hydrogen bond interaction between α1Arg92 and either β2Gln39 or β2Glu43 in RR2 or R2 is missing in R and R3 (Table 2). Interestingly, each liganded structure has four direct hydrogen bond interactions at the α1β2 dimer interface versus five in the T structure. Note that there are significant differences in other interdimer interactions (α1α2 and β1β2 dimer interfaces) among the structures, which will be discussed later.

Baldwin and Chothia (*3*) quantified the allosteric movement between the T and R Hb structures as rigid-body screw rotation, which is defined in terms of screw rotation angle, screw rotation translation, the direction of the screw rotation axis, and a point on the rotation axis. The same procedure was also used here to characterize the change in quaternary structure between pairs of the five Hb structures described above by superimposing the Cα atoms of α1β1 dimers on the BGH frame (*3*). Then, the rms deviation and the rigid-body screw rotation between the nonsuperimposed α2β2 dimers were determined. Also, as a measure of quaternary variation, the complete α1β1α2β2 tetramers were superimposed on each other using all Cα atoms (with the exception of three residues at the N- and C-termini). Before the superposition, the structures were transformed to a standard orientation in which the 2-fold dyad axes through the central water cavity were positioned along the *y*-axis with the T structure as a reference. ALIGN (*35*) and LSQKAB as implemented in the CCP4 program suite (*36*) were used for these calculations, and the results are reported in Table 3.

As expected, there are only small deviations between the superimposed α1β1 dimers of the different Hb structures (rmsd of 0.3−0.65 Å; not shown in Table 3), indicating very similar tertiary structures with the exception of significant structural differences at the EF corner−F helix−FG corner region, as well as the N- and C-termini. Notably, in the α1 subunit, there is a concerted movement of the EF corner−F helix−FG corner region in the liganded structures toward both the interdimer interface and the central water cavity relative to the T structure, with R3 showing the most shift (see below for further discussion, as well as the α1 subunit of Figure 1). In contrast to the tertiary structure analysis, the quaternary indices show all four liganded Hb structures to be conformationally different from the T structure and

Table 3: Quaternary Structure Differences of Hb Structures[a]

transition	$\alpha1\beta1\alpha2\beta2$ (Å)[b]	$\alpha2\beta2$ (Å)[c]	screw-rotation axis direction [α, β, γ (deg)][d]	screw-rotation axis point (Å)[d]	screw-rotation angle (deg)/translation (Å)[d]
T → R	2.3	5.1	28.3, 90.0, 61.7	−12.0, 10.8, −6.1	13.6/1.2
T → RR2	2.9	7.1	43.7, 89.1, 46.3	−9.1, 9.4, −7.9	17.8/2.6
T → R3	3.5	7.3	10.8, 90.0, 72.2	−14.5, 9.7, −2.6	22.0/1.7
T → R2	3.3	8.6	56.4, 89.1, 33.6	−5.6, 5.2, −7.6	23.0/3.1
T → 1FSX	2.3	5.2	47.5, 88.1, 42.6	−7.9, 10.9, −8.4	13.8/2.3
T → 1G09	2.5	5.4	34.8, 89.9, 55.2	−10.3, 8.7, −7.3	15.7/1.6
T → 1G08	2.4	5.4	50.8, 90.0, 39.2	−6.7, 11.0, −8.0	14.3/2.3
T → 1HAB	2.3	5.0	48.7, 86.8, 41.5	−7.7, 10.4, −8.4	13.9/1.8
T → 1HAC	2.3	5.1	51.3, 86.2, 40.0	−7.2, 10.0, −8.3	14.2/1.9
T → 1A9W	2.9	7.2	53.5, 87.7, 36.6	−6.6, 6.1, −7.8	19.3/2.9
R → RR2	1.0	2.5	79.0, 89.2, 11.0	−1.9, 2.6, −3.1	5.9/1.1
R → R2	1.6	4.6	85.9, 89.1, 4.2	−0.3, 0.9, −1.7	12.1/1.5
R → R3	1.6	3.2	14.5, 89.9, 75.5	−13.1, 7.3, 3.4	10.2/1.1
R → 1FSX	1.0	1.8	62.8, 88.6, 27.2	−2.0, 0.6, 5.4	4.9/0.9
R → 1G09	0.7	1.2	71.2, 86.0, 19.3	−0.5, 2.5, −5.2	3.7/0.1
R → 1G08	1.1	2.1	65.2, 88.5, 24.9	−1.3, 2.5, 5.3	6.0/1.1
R → 1HAB	1.0	1.8	54.4, 84.1, 36.2	−4.4, 3.4, 5.9	4.6/0.8
R → 1HAC	1.1	1.9	54.2, 83.2, 36.6	−5.0, 4.4, 5.4	5.3/0.9
R → 1A9W	1.4	3.4	88.2, 86.9, 3.6	−0.6, −0.2, −0.1	8.8/1.0
RR2 → R2	1.0	2.3	88.4, 89.7, 1.6	0.7, 1.1, 0.2	6.2/0.4
RR2 → R3	1.9	4.4	42.7, 88.6, 47.3	−8.3, 4.4, 6.5	12.1/1.3
RR2 → 1FSX	0.9	1.5	28.6, 89.6, 61.4	−16.2, −4.6, 3.9	4.0/−0.5
RR2 → 1G09	0.8	1.5	85.1, 84.0, 7.8	−6.5, 2.6, −0.9	2.9/1.1
RR2 → 1G08	0.9	1.5	74.2, 85.0, 15.0	−14.8, −2.6, 4.0	4.0/1.3
RR2 → 1HAB	0.9	1.7	63.0, 85.4, 26.6	−11.6, 4.6, −4.1	4.5/0.8
RR2 → 1HAC	1.0	1.7	71.1, 84.0, 17.8	−12.3, 6.0, −3.4	4.4/0.9
RR2 → 1A9W	0.9	1.3	65.3, 82.4, 25.9	−1.42, 2.4, 5.5	3.4/−0.1
R2 → R3	2.5	6.3	58.3, 88.8, 31.7	−4.4, 4.7, 6.9	17.0/1.5
R2 → 1FSX	1.3	3.3	65.5, 88.2, 24.5	−3.3, 1.1, −4.8	8.4/0.7
R2 → 1G09	1.4	3.4	88.7, 85.2, 5.0	−2.2, 1.8, −0.2	8.4/1.4
R2 → 1G08	1.3	3.2	61.1, 85.5, 29.3	−4.8, −0.8, −4.9	7.7/0.8
R2 → 1HAB	1.3	3.6	64.8, 88.4, 25.3	−26.2, −0.7, 5.9	9.0/−1.0
R2 → 1HAC	1.3	3.5	61.5, 87.6, 28.6	−2.8, 0.5, −5.9	8.7/1.0
R2 → 1A9W	0.7	1.2	62.0, 88.6, 28.0	−1.6, 8.3, −3.5	3.2/0.4

[a] See the text for a detailed description of the structural comparison and the Hb structures used for the calculations. [b] The Hb $\alpha1\beta1\alpha2\beta2$ tetramer superimposed to obtain the rms deviation. [c] The $\alpha1\beta1$ dimers superimposed, and the rms deviation of the nonsuperimposed $\alpha2\beta2$ obtained. [d] The $\alpha1\beta1$ dimers superimposed, and the rigid-body screw rotation obtained.

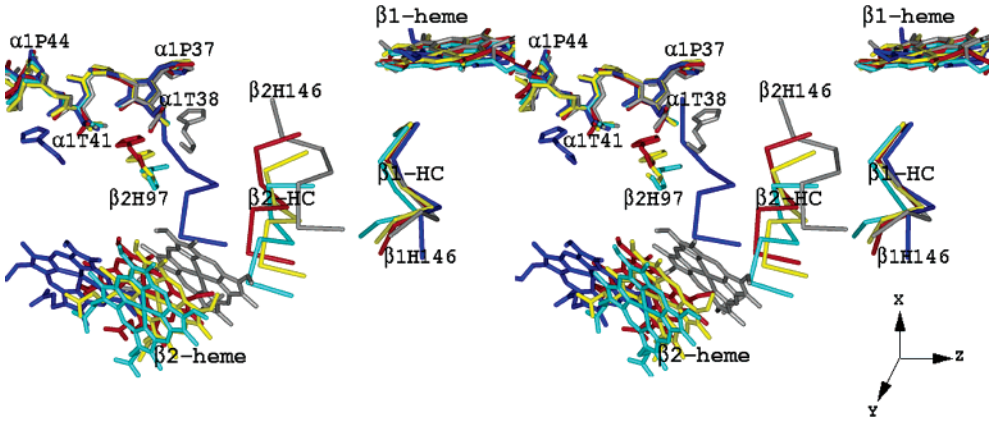

FIGURE 2: Detailed stereoview of part of the switch region, the β-cleft, and the β-heme of T (blue), R (red), RR2 (yellow), R2 (cyan), and R3 (gray) structures. The figure reveals the unusual structural characteristics of the R3 structure, as well as the intermediate structural characteristics of the RR2 structure. The structures were superimposed with the $\alpha1\beta1$ dimer as described in the text.

also from each other, with R closest to T, followed by RR2 and lastly R3 and R2 structures (see Table 3 and the $\beta2$ subunit in Figure 1). Among the liganded structures, RR2 is conformationally closest to R, followed by R3 and lastly R2. Likewise, R is the closest to R3, followed by RR2 and lastly R2. The analysis also suggests that RR2 lies in the pathway of the R → R2 transition, while R3 is an end state. Finally, the T → R3 transition is approximately in the same direction but beyond the T → R transition, while the T → RR2 (or R → RR2) transition is also approximately in the same direction but precedes the T → R2 (or R → R2) transition (see Figure 2).

Other liganded structures, including Gower II COHb (PDB entry 1A9W), bovine COHb (PDB entries 1G08 and 1G09), and cross-linked COHbA (PDB entries 1HAB and 1HAC), have been proposed to represent allosteric intermediates of the R → R2 transition (*11*−*13*). These structures, as well as another bovine COHb structure (PDB entry 1FSX), were compared with the T, R, RR2, R2, and R3 Hb structures (Table 3). The results show that the quaternary structures of

Gower II COHb, bovine COHb, and cross-linked COHbA are similar to the RR2 Hb structure, suggesting that RR2 represents a stable allosteric intermediate conformer in the R → R2 transition.

The quaternary differences, as well as the allosteric transitions between the T, R, RR2, R2, and R3 Hb structures, are best captured in Figure 2, which shows a detailed view of part of the switch region, the β-cleft, and the β-heme. In all instances, the allosteric switch from the T structure to the liganded structures has moved the β2 subunit parallel along the α1 subunit (approximately in the direction of the *z*-axis) toward the central water cavity. Accordingly, T structure residue β2His97, which lies between α1Pro44 and α1Thr41, has now moved a turn to lie between α1Thr41 and α1Thr38 in the R, RR2, and R2 structures. In the R structure, β2His97 forms a diagnostic hydrogen bond with α1Thr38; however, in RR2 and R2, the β2 subunit has further rotated ~1.1 and ~2.2 Å, respectively, in a perpendicular fashion from the α1 subunit (approximately along the *x*-axis), resulting in the disengagement of this hydrogen bond, while other switch−interface hydrogen bonds found in the R structure are maintained (Table 2). Note that the shift by RR2 places this structure between the R and R2 structures and in the same allosteric direction as R2. As a result of the allosteric shift, the switch interfaces of both RR2 and R2 have now become larger, and as previously noted in the R2 structure (*5*), two water molecules have moved into the now opened α1β2 dimer interface of the RR2 structure. The water molecules are almost in identical positions in both the RR2 and R2 structures where they mediate hydrogen bond interactions between the two subunits. It seems that these two water molecules are also present in the R structure (PDB entry 1AJ9), but each is located ~1.4 Å from the respective RR2 or R2 water molecule positions, in the same direction as the RR2 → R or R2 → R transition.

Remarkably, in the R3 structure, the β2 subunit has shifted almost a further half-turn from the R position (approximately one and one-half turns from the T position) parallel along the α1 subunit, bringing β2His97 to pack between α1Thr38 and α1Pro37, where the side chains of β2His97 and α1Pro37 make close hydrophobic contacts (Figure 2). Furthermore, the R state diagnostic hydrogen bond interaction between OG1 of α1Thr38 and O of β2His97 (2.4 Å) that was abolished in both RR2 and R2 structures is now re-formed in the R3 structure as β2His97 moves to the other side of α1Thr38. The side chain of α1Thr38 seems to occupy two alternate positions, with both conformers capable of interacting with the amide oxygen of β2His92 (2.4 or 3.2 Å). As a result of the extensive parallel shift of the R3 β2 subunit at the switch interface, the β2 subunit structural elements that form the β-cleft have moved substantially toward the central water cavity (~6−13 Å), and closer to their β1 subunit counterparts (Figures 2 and 3). This includes the C-terminus (H helix−HC segment, residues 132−146), the N-terminus (NA segment, residues 1−4), and the EF corner−F helix region (residues 79−95). The position of the C-terminal residues in R3 has resulted in pairs of symmetry-related dyad hydrogen bond interactions involving β1Ala142 and β2Asn139 (3.2 Å) and β1Asn139 and β2Asn139 (3.2 Å) that have effectively shut the β-cleft in the R3 structure (Figure 3B). In comparison, the corresponding β-cleft structures of R, RR2, and R2 have only moved approximately half as much as those of the R3, precluding the formation of the extensive β-cleft interactions observed in the R3 structure. Interestingly, in both RR2 and R2, the β2 cleft structural elements described above have shifted parallel relative to the β1 cleft elements by approximately one or two residues in the N-terminal direction of β2-HC (along the *x*-axis) compared to the R or R3 structure. This shift is a consequence of the perpendicular rotation of the RR2 and R2 β2 subunit at the switch interface (see above), leading to the two symmetry-related residues (each βHis146) moving closer toward each other. Consequently, the size of the β-cleft in RR2 and R2 has decreased relative to that of the R structure. In the R2 structure, the result is a face-on stacking interaction between the two βHis146 side chains, while RR2 with a slightly bigger space between the histidines has a phosphate molecule sitting at the dyad axis. The phosphate which overlaps the T state 2,3-DPG binding site (*32*, *33*) makes strong hydrogen bond interactions (2.8−3.1 Å) with the side chains of βHis143 and βHis146. The recently published R structure (PDB entry 1LJW) also contains a similarly bound phosphate molecule. It has been reported that 2,3-DPG binds to the same site in the deoxygenated or oxygenated Hb β-cleft (*37*, *38*), consistent with the crystallographic observations described above. It is highly unlikely that a phosphate molecule or for that matter an allosteric effector can bind to the β-cleft of R3 structure due to the smaller β-cleft, as well as the intersubunit hydrogen bond interactions that have completely closed the cleft. The β-cleft in R2, although bigger than that of R3, may also not be able to accommodate a phosphate molecule, unless there is a rearrangement of the βHis146 side chains or the C-termini.

Preferential binding of 2,3-DPG to the wider β-cleft of the T structure stabilizes the quaternary structure of this state with a concomitant decrease in oxygen affinity. The expulsion of 2,3-DPG due to the narrowing of the β-cleft also leads to the formation of the R conformation, increasing the oxygen affinity of Hb. The fact that liganded Hbs are capable of binding effectors could lead to a reduction in Hb oxygen affinity, and since these structures may have different affinities for the effector because of differences in β-cleft size, it is quite conceivable that they would also exhibit different affinities for oxygen, most likely with R3 showing the highest and R the lowest. This is consistent with COHbA structure 1LJW having T state characteristics caused by a bound phosphate at the β-cleft (*34*). As we will discuss later, the different β-cleft sizes may also affect diffusion of chloride and other ions into the central water cavity which could have an impact on Hb oxygen affinity.

In general, the quaternary differences at the α-cleft of the liganded structures are significantly smaller than those observed at the β-cleft, and like the latter, the N-terminal (NA), EF corner−F helix, and C-terminal (HC) residues at the α-cleft of the R3 structure have moved closer to the dyad axis from the T structure position by ~1−4 Å (Figure 4A). In contrast, the other liganded structures have only moved very little from the T position. As observed at the β-cleft, the position of the N-terminal NA segment and the C-terminal H helix−HC segment in the R3 structure at the α-cleft have also resulted in extensive pairs of symmetry-related dyad hydrogen bond interactions involving α1Val1 and α2Ser138 (2.8 Å), α1Val1 and α2Lys139 (3.0 Å),

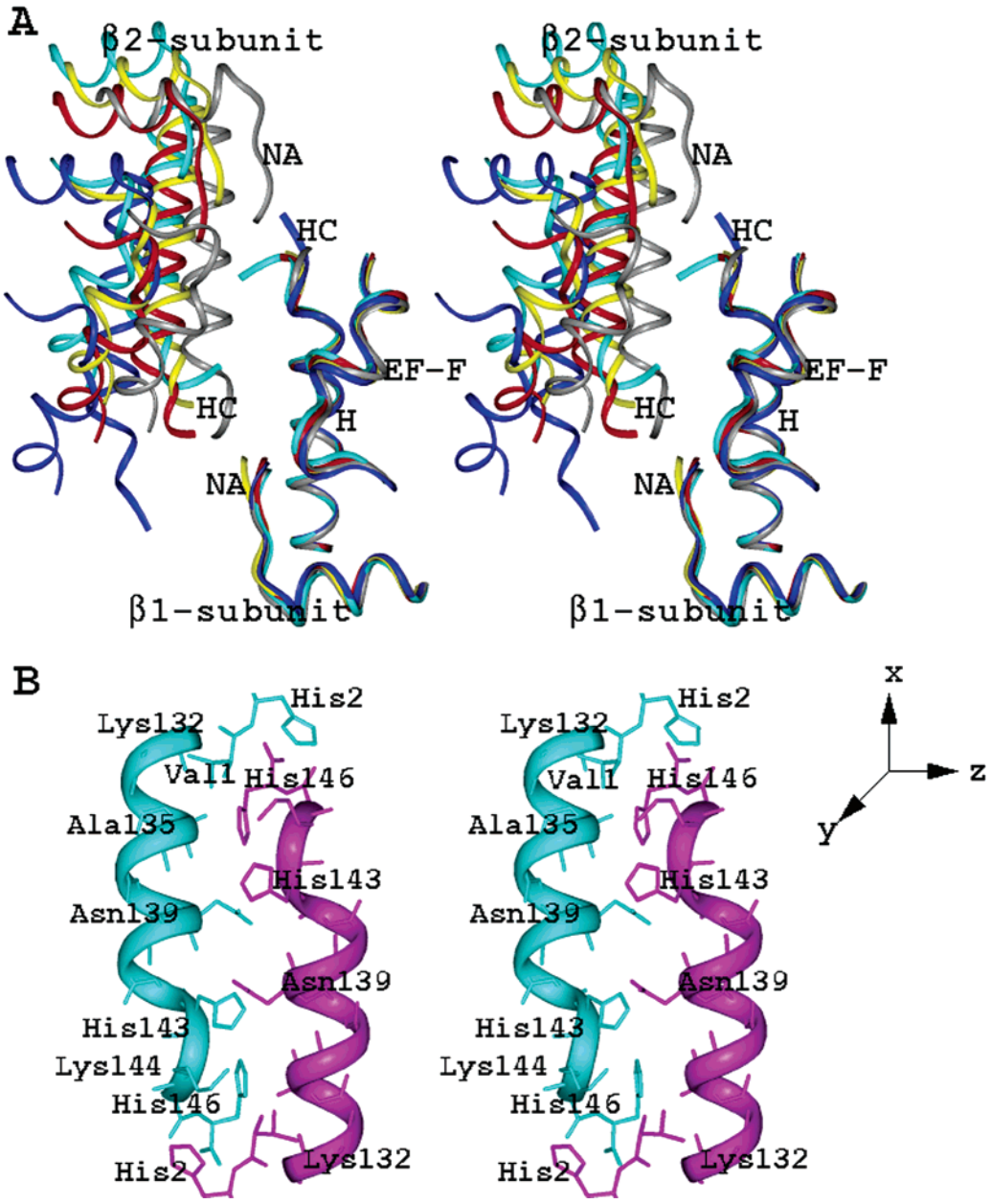

FIGURE 3: Stereofigure of the β-cleft. (A) Superposition of T (blue), R (red), RR2 (yellow), R2 (cyan), and R3 (gray) structures showing the NA segment, A helix, F helix, H helix, HC segment, and N- and C-terminal residues. All structural elements occur in pairs related by the dyad axis of symmetry (*y*-axis), which is perpendicular to the plane of the page. The structures were superimposed with the $\alpha 1\beta 1$ dimer as described in the text. (B) Pairs of symmetry-related dyad hydrogen bond interactions involving the H helix−HC segment of the R3 structure.

α1Val1 and α2Arg141 (2.7 Å), α1Leu2 and α2Arg141 (3.2 Å), α1Ser131 and α2Arg141 (2.5 Å), and α1Thr134 and α2Arg141 (3.2 Å) (Figure 4B). The first three interactions are conserved in the R structure. In contrast, none of these interactions are found in either the RR2 or R2 structure due to the fact that the symmetry-related HC segments have shifted in a parallel manner away from each other by almost two residues toward the C-terminal direction of the α2-HC segment (along the *x*-axis) compared to the R or R3 position. This has resulted in the two α-subunit αArg141 residues moving farther apart in RR2 and R2, leading to the apparent disordering of the αArg141 residue in these structures, especially RR2 which has no observed density at residues αTyr140 and αArg141. It should be recalled that a similar parallel shift occurred at the β-clefts of RR2 and R2, but in the opposite direction which resulted in the two βHis146 residues moving closer to each other. Interestingly, a new hydrogen bond interaction has formed across the dyad between αLys127 and αLys139 in both RR2 and R2 structures due to the α2−HC segment shift. This hydrogen bond is absent in the R and R3 structures. The relatively larger α-cleft in R2 compared to those in both R and R3 explains why in a recent study (*39*) small aldehyde antisickling compounds were found bound preferentially to the α-cleft of the R2 structure (see below for further discussion).

Heme Environments. All hemes are fully ligated in the liganded structures, as indicated by *B*-factors comparable with those of the rest of the heme atoms. We assume the hemes to be significantly if not 100% CO-bound since the irons were fully reduced with $Na_2S_2O_4$ prior to addition of CO. In addition, the crystallization tube was kept under a CO atmosphere. The iron atoms are centered in the porphyrin

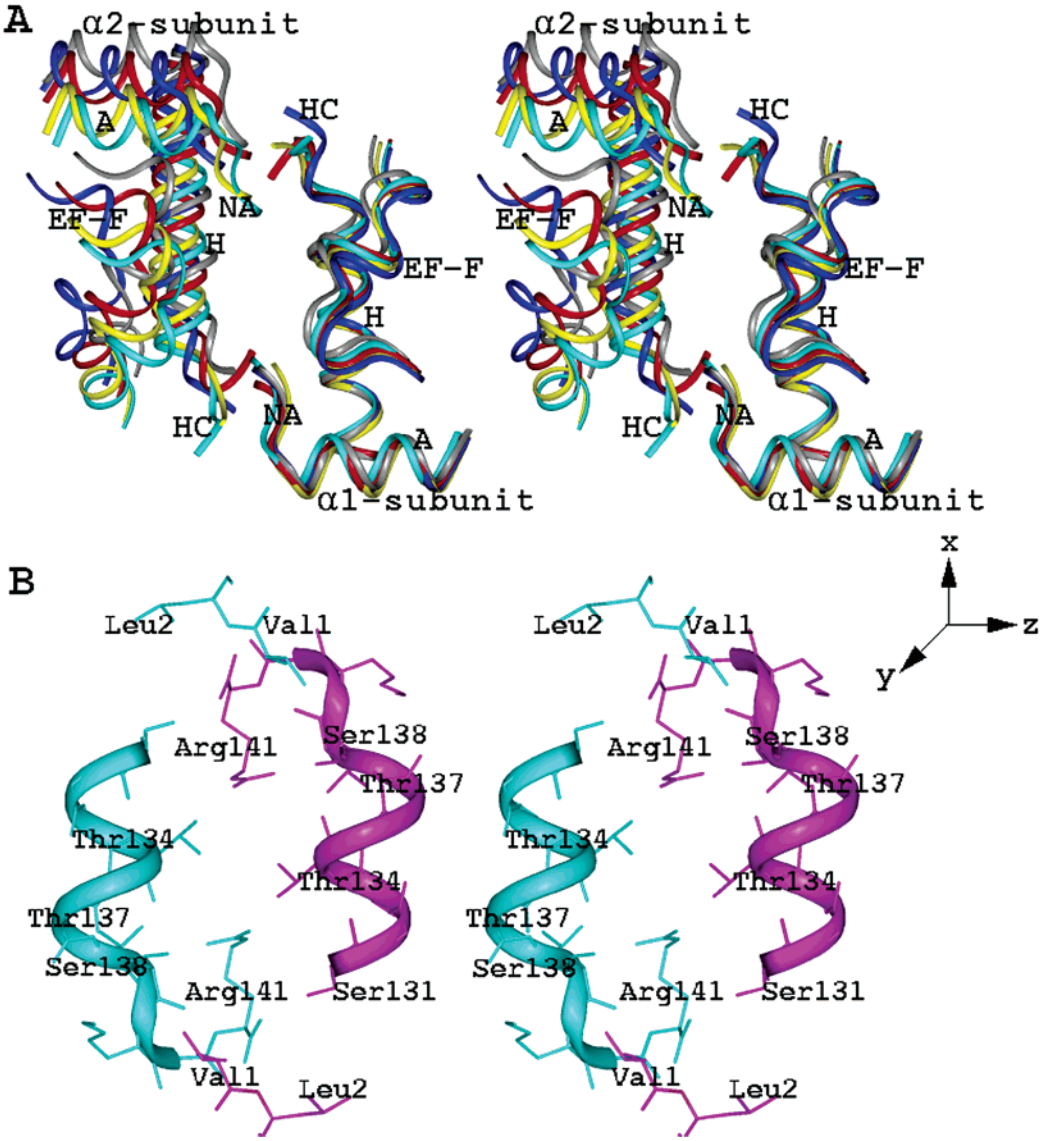

FIGURE 4: Stereofigure of the α-cleft. (A) Superposition of T (blue), R (red), RR2 (yellow), R2 (cyan), and R3 (gray) structures showing the NA segment, A helix, F helix, H helix, HC segment, and N- and C-terminal residues. (B) Pairs of symmetry-related dyad hydrogen bond interactions involving the NA segment and the H helix−HC segment of the R3 structure.

Table 4: Geometry and Environment of Heme Groups in the R, RR2, R2, and R3 Hb Structures[a]

	R		RR2				R2				R3	
	α1	β1	α1	α2	β1	β2	α1	α2	β1	β2	α1	β1
Fe−His(F8) NE2	2.05	2.02	2.03	2.01	2.08	2.07	2.08	2.13	2.10	2.10	1.99	2.06
$\langle Fe-N_{porph}\rangle$[b]	2.01	2.02	2.01	2.02	2.03	2.01	2.00	2.03	2.00	2.00	2.04	2.08
Fe−C	1.85	1.81	1.91	1.83	1.80	1.76	1.77	1.78	1.77	1.75	1.76	1.89
Fe−Val(E11) CG2	5.04	4.52	4.70	4.97	4.81	4.98	4.80	4.96	4.87	4.97	4.95	5.06
Fe−Ct[c]	−0.02	0.00	−0.06	0.00	0.05	0.00	0.00	0.00	−0.01	−0.02	0.00	−0.07
C−Val(E11) CG2	3.72	3.33	3.52	3.76	3.45	3.51	3.70	3.57	3.71	3.58	3.85	3.77
O−Val(E11) CG2	3.14	3.06	3.13	3.38	3.01	3.09	3.20	3.38	3.19	3.20	3.17	3.65
C−His(E7) NE2	3.44	3.40	3.39	3.42	3.51	3.44	3.47	3.49	3.40	3.56	3.49	3.92
O−His(E7) NE2	3.30	3.24	3.20	3.43	3.47	3.40	3.23	3.30	3.19	3.27	3.24	3.97
Fe−C−O	177	173	178	173	170	159	173	156	172	163	162	162

[a] Distances and angles are in angstroms and degrees, respectively. [b] Average distance between Fe and the four porphyrin nitrogens. [c] Distance from the Fe to the least-squares fit plane of the porphyrin nitrogens.

planes. At the proximal side of the α- and β-heme pockets, stereochemical parameters between the proximal histidine and the heme are similar in all the structures. Also, at the distal heme pockets, the ligand environments are similar, with the exception of a significant lengthening of the nonbonded contacts between the β-heme distal residues and the CO ligand in R3 compared to the other structures (Table 4; discussion below).

Superposition of the BGH frame of the α1β1 dimer reveals large tertiary structural differences at the α-heme in the positions of the EF corner, F helix, and FG corner (α1 subunit of Figure 1 and Figure 5A). As pointed out earlier,

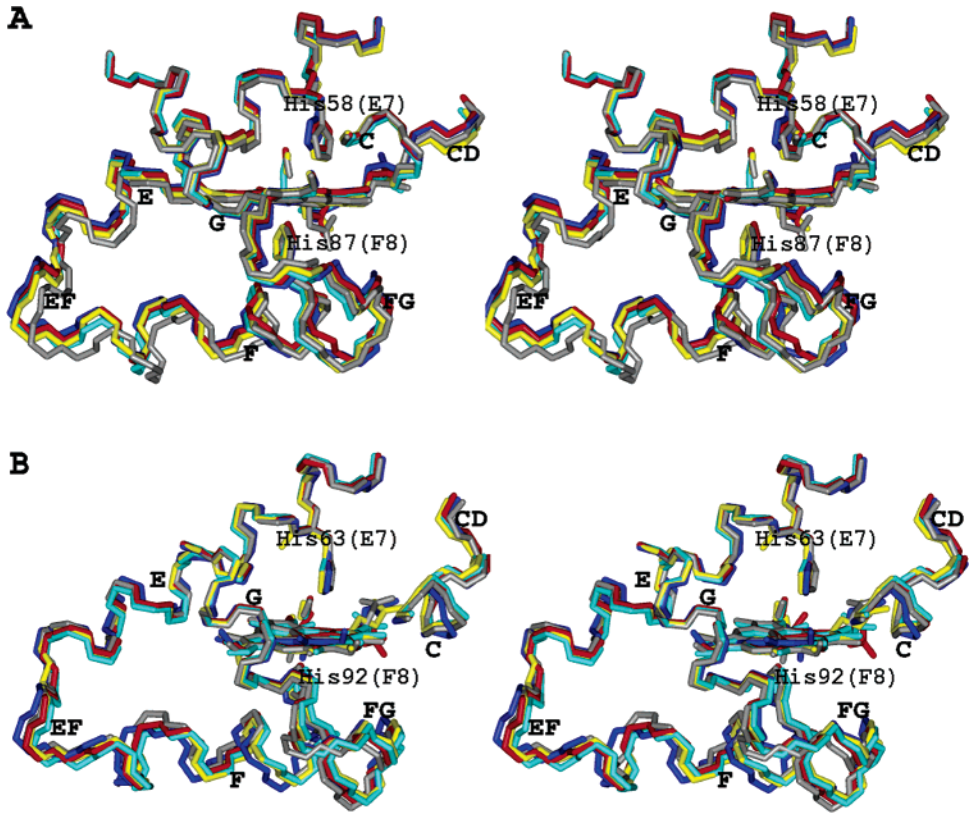

FIGURE 5: Stereofigure of the β-subunit showing the heme, bound ligand, C helix, CD corner, E helix, F helix, and FG corner of T (blue), R (red), RR2 (yellow), R2 (cyan), and R3 (gray) structures. The structures were superimposed with the $\alpha 1\beta 1$ dimer as described in the text: (A) $\beta 1$ subunit heme group and environment and (B) $\beta 2$ subunit heme group and environment.

in all the liganded structures, there is a concerted movement of these structural elements toward both the interdimer interface and central water cavity relative to the T structure, with R3 exhibiting the largest shift. Perutz (*1*, *2*) attributed the low oxygen affinity of the T state to the tension of the proximal histidine restraining the movement of the iron atom from its out-of-plane position in the T structure to its in-plane position in the R structure. He further showed that movement of the αF helix and αFG corner residues toward the central water cavity from the T to R position led to relaxation of the strain with a concomitant increase in oxygen affinity. The position of the αF helix−αFG corner residues in R3 indicates a more reduced strain at the α-heme compared to the other liganded structures and should translate to R3 exhibiting the highest affinity for oxygen among the liganded Hbs.

Although the corresponding β-heme structures show significant differences from the T positions, unlike those in the α-subunit the differences among the liganded structures are small and do not follow any obvious trend (Figure 5B). However, one of the most distinctive structural features observed in the R3 structure is a hydrogen bond interaction between one of the β-heme propionates and the imidazole side chain of the distal histidine (3.2 Å). Apparently, this interaction has perturbed the E helix, and as a result, the side chains of Val67 (E11) and His63 (E7) have moved significantly away from the CO ligand (0.3−0.65 Å), when compared to the other liganded structures (Table 4). As pointed out by Perutz (*1*), steric hindrance to ligand binding by the distal residues is dominant in β-heme and is a factor contributing to the low oxygen affinity of the T state. Hence, the reduced steric contact between the ligand and the distal residues in R3 may greatly enhance the affinity for oxygen at the β-heme of R3 state Hb compared to the other liganded Hbs.

Table 5: Iron−Iron Distances in the T, R, RR2, R2, and R3 Hb Structures

hemoglobin	$\alpha 1\beta 1^a$	$\alpha 1\beta 2^a$	$\alpha 1\alpha 2$	$\beta 1\beta 2$	total
T	36.5	24.4	34.2	39.5	134.6
R	34.8	25.7	34.8	34.7	130.0
R2	34.5	26.1	35.2	34.3	130.1
RR2	34.3	26.1	35.0	33.6	129.0
R3	34.1	26.2	33.3	30.7	124.1

[a] Distance averaged between the two symmetry-related dimers for the structures with a tetramer in the asymmetric unit.

Iron−Iron Distances. Remarkably, the nature of the allosteric transitions has also brought about significant differences in the heme−heme distance and geometry in the Hb structures (Table 5). While the corresponding $\alpha 1$Fe−$\beta 2$Fe, $\alpha 1$Fe−$\beta 1$Fe, $\alpha 1$Fe−$\alpha 2$Fe, and $\beta 1$Fe−$\beta 2$Fe distances are fairly constant in R, RR2, and R2 structures, they differ significantly from those of the T and R3 structures, most notably the $\beta 1$Fe−$\beta 2$Fe distance. In the T and R3 structures, the $\beta 1$Fe−$\beta 2$Fe distance has become the longest and shortest, respectively. This is due to the parallel shift of the T structure $\beta 2$ subunit along the $\alpha 1$ subunit by a turn in R, RR2, and R2, and almost one and one-half turns in R3 that has brought the $\beta 1$ and $\beta 2$ subunits closer together in the liganded Hbs. The T structure shows the largest total Fe−Fe distance (∼135 Å), followed by the three liganded structures, R, RR2, and R2, with very similar distances (∼130 Å), and lastly the R3 structure (124 Å). Most interesting is the difference in the total Fe−Fe distance of the T structure and the three liganded

structures, R, RR2, and R2 (~5 Å), which is almost similar in magnitude to the difference in the Fe−Fe distance of the R3 structure, and the other liganded R, RR2, and R2 structures (~6 Å).

The different heme−heme distances have resulted in variation in the relative arrangement of the four hemes, which change from very unsymmetrical in the T structure, to symmetrical in the R structure, to slightly unsymmetrical in RR2 and R2 structures, and to very unsymmetrical in the R3 structure. This may be biologically significant as the T structure with the most widened β-cleft binds 2,3-DPG, while the R3 structure with the smallest β-cleft may be completely precluded from binding 2,3-DPG. On the other hand, R, RR2, and perhaps R2 with a varying intermediate β-cleft size may bind 2,3-DPG, albeit more weakly, as suggested by this study and others (*34*, *37*, *38*). In effect, the different liganded structures may exhibit different affinities for oxygen, depending on the size of the β-cleft.

Central Water Cavity and Chloride Effect. Positively charged residues in the central water cavity are believed to partially account for the Bohr effect in Hb (*40*, *41*), which is attributed to specific preferential binding of chloride ions to these charges (*42*, *43*). Other studies, however, suggest that chloride ions rather move freely to neutralize the excess positive charges in the central water cavity (*44*−*46*). The effect is greater in the T structure because of the larger central water cavity, leading to greater stabilization of the T state relative to the relaxed state. As already pointed out, the β-cleft entrance to the central water cavity in the R3 structure has become narrowed and completely blocked by hydrogen bond interactions across the dyad axis, while the entrance at the α-cleft is significantly reduced compared to those of the other liganded structures. The smaller entrance to the water cavity in the R3 structure should impede diffusion of chloride ions into the cavity, and should translate to a higher oxygen affinity in R3 state Hb compared to the other liganded Hbs. R, RR2, and R2 state Hbs may also have varying oxygen affinities due to the fact that the sizes of both the α- and β-clefts are different in these Hbs. Interestingly, R3 has the fewest water molecules observed in the central water cavity among the liganded structures, even when compared to other liganded Hb structures with a similar resolution of ~2.1 Å.

As noted above for the RR2 and R3 structures, the regions encompassing the β-subunit N-terminus, C helix−CD corner region, E helix−EF corner−F helix−FG corner region, and C-terminus, as well as the β-heme of all the liganded structures, are characterized by high *B*-factors, compared to the average *B*-factor of the protein or the analogous α-subunit structures, with R3 showing the most flexibility. The structural elements described above form an envelope around the β-heme, and also form part of the β-cleft. Of interest is the fact that in some of the liganded structures, even though the above regions are involved in crystal packing, they are still flexible. It could be that this flexibility may be physiologically important, by playing a dynamic role in closing and opening the central water cavity via the β-cleft, as well as modulating the size of the distal β-heme pocket.

Proposed Allosteric Pathways. The crystallization experiments clearly indicate that different liganded Hb structures are in equilibrium with each other. Also, the structural analysis undoubtedly points to R3 as an end state, while RR2 is an intermediate in the R → R2 transition. Silva et al. (*5*) and Smith et al. (*6*, *7*) have previously suggested that a direct T → R transition would be impossible due to a steric barrier between β2His97 and α1Thr41. To overcome this barrier, the authors suggested that the T structure has to open up first and cause a conformational change to the R2 structure, which then rotates to assume the R conformation. However, other studies rather suggest R2 is an end state (*8*−*11*). Most notable is that of Srinivasan and Rose (*10*), who showed through computational analysis that the T → R2 → R pathway suggested by Silva and Smith (*5*−*7*) is geometrically impossible and further demonstrated that a direct T → R transition can occur without any steric barrier because of α1 and β2 subunit motions that are in mutually opposite directions. On the basis of our structural analysis as well as other previous studies (*8*−*11*), we propose that both R2 and R3 structures are two extreme relaxed end states. Second, the R structure is acting as an intermediate in the T → R3 transition, while the T → R2 transition is mediated by both R and RR2 structures. Finally, the R → R3 transition most probably occurs without the compound passing through either the RR2 or R2 structure. The proposed allosteric pathways between the different Hb states are depicted in Figure 6.

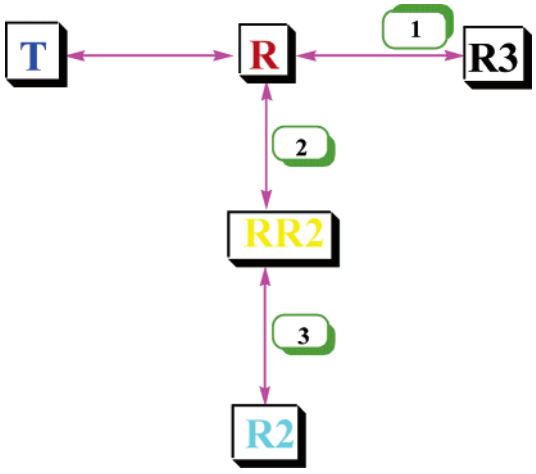

FIGURE 6: Schematic representation of the proposed allosteric pathway between the different Hb states. This study, as well as others (see the text), suggests the most probable pathway to be that denoted by the red arrows, where both R2 (cyan) and R3 (black) are liganded end state structures. The transition between T (blue) and R2 is mediated by R (red) and RR2 (yellow), while the transition between T and R3 is mediated by R. The R → R3 transition is supported by the crystal structures of two other R3-like structures (unreported data from our laboratory, denoted by 1) that lie in the R to R3 pathway. The R → R2 transition is supported by the cross-linked COHbA (PDB entries 1HAB and 1HAC), bovine COHb (PDB entries 1FSX, 1G08, and 1G09) with quaternary structures intermediate between those of R and RR2 (denoted by 2) and Gower II COHb (1A9W) between RR2 and R2 (denoted by 3).

It is quite possible that there are other intermediate structures between R and RR2 structures, as well as between RR2 and R2 structures that are yet to be discovered for normal human Hb. This is clearly suggested by the structures of cross-linked COHbA (PDB entries 1HAB and 1HAC), bovine COHb (PDB entries 1FSX, 1G08, and 1G09) that are found to have intermediate conformations between the R and RR2 structures. Likewise, Gower II COHb (PDB entry 1A9W) is also found to have intermediate structural conformation between RR2 and R2 structures (see Table 3). On the other hand, it is unlikely for any other liganded structures

beyond R3 to exist, if it involves further shifting of the β2 subunit (along the *z*-axis) toward the central water cavity because of severe steric clashes between the two symmetry-related H helix−HC segment residues that form the β-cleft (see Figures 2 and 3).

It seems that breaking of the hydrogen bond between β2His97 and α1Thr38 in the R structure may be part of a process that causes conformational changes at the R structure $\alpha1\beta2$ dimer interface, leading to formation of the T, RR2, or R3 structure. This inference is substantiated by the R COHbA (PDB entry 1LJW) structure that shows considerable weakening of the β2His97−α1Thr38 hydrogen bond, which the authors attributed to an initiation of the allosteric transition from the R state to the T state (*34*). This hydrogen bond is still observed in the R3 structure (2.4 or 3.2 Å as described above), but of particular interest is the fact that two other refined R3 structures (unpublished results from our laboratory) show significantly different bond contacts between β2His97 and α1Thr38 (3.8 and 4.4 Å). This is due to the varying degree of the parallel shift of the β2 subunit relative to the α1 subunit, with the R3 structure reported here showing the most shift from the R position. As a result, we see a subtle but significant gradation of conformational changes along the R → R3 transition. For example, the β1Fe−β2Fe distance varies from 30.6 Å (R3 structure reported here) to 31.9 and 32.6 Å (in the two other R3 structures), and as expected, the β-cleft is slightly looser in those R3 structures with longer $\beta1-\beta2$ iron−iron distances. This observation is significant in suggesting that a direct R → R3 transition is possible without the two subunits necessarily rotating apart, but through mutual parallel subunit rotation motions as suggested for the T → R transition (*10*).

Although possible, but highly unlikely, a T → R3 transition mediated by all three R, RR2, and R2 structures cannot be ruled out. That is, after disengagement of β2His97 and α1Thr38 in the R structure, the β2 subunit, instead of shifting parallel to the R3 position, rather moves perpendicularly away from the α1 subunit through the RR2 structure to the R2 structure, which then rotates back to assume the R3 structure. Indeed, as Figure 2 shows, the transition from R to R2 seems to take the β2 subunit toward the R3 position. Arguing against this pathway is the gradation of R3 structures along the R → R3 shift that suggests that the transition occurs through mutual parallel subunit rotation motions. Moreover, it seems that the R structure is geometrically closer to the R3 structure than either the R2 or RR2 structure to the R3 structure.

Physiological Relevance. For more than three decades, the T and R structures provided the basis for explaining Hb allosterism (through either the MWC or the KNF model), and most of the functional properties associated with the allosteric transition between the tense and relaxed states. The discovery of the R2 structure (*5*−*7*) and quite recently RR2-like structures (*11*−*13*, *17*) has resulted in rethinking of the earlier allosteric views to take into account these new liganded Hb structures.

Safo et al. (*39*) recently showed that R2 crystals could be formed from a deoxygenated HbA solution cocrystallized with antisickling agents (aromatic aldehydes) using high-salt conditions [3.2−3.6 M sulfate/phosphate precipitant (pH 6.5)]. Interestingly, this R2 complex structure (PDB entry 1QXD or 1QXE) is indistinguishable from the native R2 structure (PDB entry 1BBB) which was crystallized from low-salt conditions (*5*). As noted by the authors, the R2 crystals appear to be formed as a result of the aldehydes binding to fully or partially ligated Hb in the form of the R2 state, in equilibrium with the predominant T Hb that eventually increased the R2 Hb fraction. The aldehydes bind to the α-cleft, forming Schiff base adducts in a symmetrical fashion with the N-terminal αVal1 nitrogens. Cocrystals of R and R3 COHbA with the aldehydes show a significantly low to nonexistent presence of the compounds, due to steric crowding at the binding sites of both R (*39*) and R3 structures (unpublished results from our laboratory). The RR2 structure, with a binding α-cleft significantly larger than that of the R2 structure, may also bind the aldehydes. However, as observed in T state Hb cocrystals (*39*), the bound effector may be delocalized due to the large binding pocket. It seems that the preferential binding of the aldehyde to the R2 structure, among the other liganded structures, led to the increased fraction of the R2 form. The presence of multiple liganded Hb states is also consistent with a laser photolysis study by Sawicki and Gibson (*47*) with COHb that shows distinct conformations of liganded Hb, and at a pH below 8.0, these liganded conformations appear to be a function of pH. Moreover, a recent NMR study at near-physiological conditions of pH, ionic strength, and temperature showed that liganded Hb exists as a mixture of R, R2, and a structure intermediate between R and R2 in solution (*48*). Most likely, this intermediate structure is similar to the RR2 structure reported here.

One current view of the Hb allosteric mechanism assumes that R2 is the physiological relaxed end state based partly on the fact that it was crystallized under low-salt conditions that mimic the in vivo environment (*10*, *11*), and that R is a modified or an intermediate state trapped between the T and R2 states by the high-salt conditions. This view is supported by Gower II COHb (*12*) and bovine COHb structures (*13*), all crystallized from low-salt conditions to give RR2- or R2-like structures. However, this study, as well as others (*14*, *39*), shows that both RR2 and R2 liganded Hbs can be crystallized using high-salt conditions. In a recent crystallization study of human methemoglobin (*17*) using low-salt and pH conditions that have been used to grow R2 and R crystals, respectively, the ensuing crystal structure showed three independent liganded Hb molecules in the asymmetric unit. Interestingly, the three molecules have quaternary structures that lie between those of the R and R2 structures, with varying degrees of closeness to these two structures. It seems that different relaxed Hb states may coexist in equilibrium either in high-salt conditions or in physiologically low-salt conditions. The cooperative free energy, which is the difference in energy of dimer-to-tetramer association of T Hb (−14.3 kcal/mol) and liganded Hb (−8.0 kcal/mol), is mostly due to the differences and strength of the $\alpha1\beta2$ interdimer contacts (*49*). The similarities in the $\alpha1\beta2$ interdimer contacts in the liganded structures suggest that the cooperative free energy of the four liganded Hbs may be very similar. Thus, the energy involved in changing one liganded form to another may be very small (*13*), and the fraction and consequent crystallization of any one form may depend on subtle differences in the crystallization conditions, which are currently not properly understood. We should therefore be cautious in attributing a particular crystal

structure to a physiological state because it crystallizes at a certain condition. Under physiological conditions in the body, liganded Hb may undergo structural and functional changes in response to subtle changes in the ionic strength, the concentration of protons, and the presence of other protein ligands and/or allosteric effectors.

The discovery of the R3 structure further complicates the liganded structure concept, and whether this novel structure, and indeed such a state, is relevant in Hb allostery would have to be considered in the context of the unusually "superrelaxed" structural properties of R3 that suggest that the transition from the T state to the relaxed state may give rise to liganded Hbs with varying Hb oxygen affinities. In various solution and crystallographic studies by Bucci et al. (*50*, *51*), the authors showed that Hb behaved like a multistate system, where each step of oxygenation has its own distinct conformation, with varying oxygen affinities. Other studies, using cryoelectrophoresis (*52*) and Raman spectroscopy (*53*), also strongly support the concept described above. Perhaps these distinct Hb structures model R, RR2, R2, R3, and other undiscovered liganded states, consistent with our analysis that suggests that the different liganded structures may exhibit different affinities for oxygen. The presence of multiple relaxed conformations is not unique to Hb. For example, aspartate transcarbamoylase, which is also an allosteric enzyme, is found to exist in multiple structural conformations in the relaxed state (*54*). Another example is the multisubunit immunoglobulin light chain protein, for which the structure has been determined in three different quaternary conformations (*55*).

While the RR2 structure easily fits into the current allosteric mechanism, the R3 structure, on the other hand, may further complicate the Hb allostery concept. We recognize that there are many unanswered questions, such as the implication of more than one relaxed end state and the physiological relevancy of the R3 structure, but we hope that this article would generate further debate on Hb allostery, which has become controversial with the discovery of the R2 structure.

REFERENCES

1. Perutz, M. F. (1970) Stereochemistry of cooperative effects in hemoglobin, *Nature 228*, 726−734.
2. Perutz, M. F. (1972) Haem-haem interaction, *Nature 237*, 459−499.
3. Baldwin, J., and Chothia, C. (1979) Haemoglobin: The structural changes related to ligand binding and its allosteric mechanism, *J. Mol. Biol. 129*, 175−220.
4. Monod, J., Wyman, J., and Changeux, J.-P. (1965) On the nature of allosteric transitions: A plausible model, *J. Mol. Biol. 12*, 88−118.
5. Silva, M. M., Rogers, P. H., and Arnone, A. (1992) A third quaternary structure of human Hb at 1.7 Å resolution, *J. Biol. Chem. 267*, 17248−17256.
6. Smith, F. R., Lattman, E. E., and Carter, C. W. R. (1991) The mutation β99 Asp-Tyr stabilizes a new composite quaternary state of human Hb, *Proteins 10*, 81−91.
7. Smith, F. R., and Simmons, K. C. (1994) Cyanomet human Hb crystallized under physiological conditions exhibits the Y quaternary structure, *Proteins 18*, 295−300.
8. Janin, J., and Wodak, S. J. (1993) The quaternary structure of carbonmonoxy Hb Ypsilanti, *Proteins 15*, 1−4.
9. Doyle, M. L., Lew, G., Turner, G. J., Rucknagel, D., and Ackers, G. K. (1992) Regulation of oxygen affinity by quaternary enhancement: Does hemoglobin Ypsilanti represent an allosteric intermediate? *Proteins: Struct., Funct., Genet. 14*, 351−362.
10. Srinivasan, R., and Rose, G. D. (1994) The T-to-R transformation in Hb: A re-valuation, *Proc. Natl. Acad. Sci. U.S.A. 91*, 11113−11117.
11. Schumacher, M. A., Zheleznova, E. E., Poundstone, K. S., Kluger, R., Jones, R. T., and Brennan, R. G. (1997) Allosteric intermediates indicate R2 is the liganded hemoglobin end-state, *Proc. Natl. Acad. Sci. U.S.A. 94*, 7841−7844.
12. Sutherland-Smith, A. J., Baker, H. M., Hofman, O. M., Brittain, T., and Baker, E. N. (1998) Crystal Structure of a Human Embryonic Haemoglobin: The Carbonmonoxy Form of Gower II (α2e2) Haemoglobin at 2.9 Å Resolution, *J. Mol. Biol. 280*, 475−484.
13. Mueser, T. M., Rogers, P. H., and Arnone, A. (2000) Interface sliding as illustrated by the multiple quaternary structures of liganded hemoglobin, *Biochemistry 39*, 15353−15364.
14. Safo, M. K., and Abraham, D. J. (2001) The X-ray structure determination of bovine carbonmonoxy hemoglobin at 2.1 Å resoultion and its relationship to the quaternary structures of other hemoglobin crystal forms, *Protein Sci. 10*, 1091−1099.
15. Fermi, G., Perutz, M. F., Shaanan, B., and Fourme, R. (1984) The crystal structure of human deoxyHb at 1.7 Å resolution, *J. Mol. Biol. 175*, 159−174.
16. Ward, K. B., Wishner, B. C., Lattman, E. E., and Love, W. E. (1975) Structure of deoxyhemoglobin A crystals grown from polyethylene glycol solutions, *J. Mol. Biol. 98*, 161−177.
17. Biswal, B. K., and Vijayan, M. (2001) Structure of methhaemoglobin: The variation of a theme, *Curr. Sci. 81*, 1100−1105.
18. Safo, M. K., and Abraham, D. J. (2003) in *Methods in Molecular Medicine: Hemoglobin Disorders, Molecular Methods and Protocols* (Nagel, R. L., Ed.) Vol. 82, p 1, Humana Press, Totowa, NJ.
19. Perutz, M. F. (1968) Preparation of Hb crystals, *J. Cryst. Growth 2*, 54−56.
20. Navaza, J. (1994) AMoRe: An automated package for molecular replacement, *Acta Crystallogr. D50*, 157−163.
21. Brunger, A. T., Adams, P. D., Clore, G. M., DeLano, W. L., Gros, P., Grosse-Kunstleve, R. W., et al. (1998) Crystallography & NMR system: A new software suite for macromolecular structure determination, *Acta Crystallogr. D54*, 905−921.
22. Cambillau, C., and Horjales, E. (1987) TOM: A Frodo subpackage for protein−ligand fitting with interactive energy minimization, *J. Mol. Graphics 5*, 174−177.
23. Perutz, M. F. (1946) The composition and swelling properties of haemoglobin crystals, *Trans. Faraday Soc. 92B*, 187−195.
24. Green, D. W., Ingram, V. M., and Perutz, M. F. (1954) The structure of haemoglobin IV. Sign determination by the isomorphous replacement method, *Proc. R. Soc. A225*, 287−307.
25. Robinson, V. L., Smith, B. B., and Arnone, A. (2003) A pH-dependent aquomet-to-hemichrome transition in crystalline horse methemoglobin, *Biochemistry 42*, 10113−10125.
26. Safo, M. K., Abdulmalik, O., Lin, H. R., Asakura, T., and Abraham, D. J. (2005) Structures of R- and T-state hemoglobin Bassett: Elucidating the structural basis for the low oxygen affinity of a mutant hemoglobin, *Acta Crystallogr. D61*, 156−162.
27. Schoenborn, B. P. (1976) Dichloromethane as an antisickling agent in sickle cell hemoglobin, *Proc. Natl. Acad. Sci. U.S.A. 73*, 4195−4199.
28. Abraham, D. J., Mehanna, A. S., and Williams, F. L. (1982) Design, Synthesis, and Testing of Potential Antisickling Agents. 1. Halogenated Benzyloxy and Phenoxy Acids, *J. Med. Chem. 25*, 1015−1017.
29. Wishner, B. C., Ward, K. B., Lattman, E. E., and Love, W. E. (1975) Crystal structure of sickle-cell deoxyhemoglobin at 5 Å resolution, *J. Mol. Biol. 98*, 179−194.
30. Benesch, R. E., Kwong, S., Benesch, R., and Edjali, R. (1977) Location and bond type of intermolecular contacts in the polymerisation of haemoglobin S, *Nature 269*, 772−775.
31. Frier, J. A., and Perutz, M. F. (1977) Structure of human foetal deoxyhaemoglobin, *J. Mol. Biol. 112*, 97−112.
32. Arnone A. (1972) X-ray diffraction study of binding of 2,3-diphosphoglycerate to human deoxyhaemoglobin, *Nature 237*, 146−149.
33. Richard, V., Dodson, G. G., and Mauguen, Y. (1993) Human deoxyhaemoglobin-2,3-diphosphoglycerate complex low-salt structure at 2.5 Å resolution, *J. Mol. Biol. 233*, 270−274.
34. Safo, M. K., Burnett, J. C., Musayev, F. N., Nokuri, S. S., and Abraham, D. J. (2002) Crystal structure of human carbonmonoxy hemoglobin at 2.16 Å: A snapshot of the allosteric transition, *Acta Crystallogr. 58*, 2031−2037.

35. Cohen, G. E. (1997) *ALIGN*: A program to superimpose protein coordinates, accounting for insertions and deletions, *J. Appl. Crystallogr. 30*, 1160−1161.
36. Collaborative Computational Project No. 4 (1994) *Acta Crystallogr. D50*, 760−763.
37. Yonetani, T., Park, S. I., Tsuneshige, A., Imai, K., and Kanaori, K. (2002) Global allostery model of hemoglobin. Modulation of O_2 affinity, cooperativity, and Bohr effect by heterotropic allosteric effectors, *J. Biol. Chem. 277*, 34508−34520.
38. Gupta, R. K., Benovic, J. L., and Rose, Z. B. (1979) Location of the allosteric site for 2,3-bisphosphoglycerate on human oxy- and deoxyhemoglobin as observed by magnetic resonance spectroscopy, *J. Biol. Chem. 254*, 8250−8255.
39. Safo, M. K., Abdulmalik, O., Danso-Danquah, R., Burnett, J. C., Nokuri, S., Joshi, G. S., Musayev, F. N., Asakura, T., and Abraham, D. J. (2004) Structural basis for the potent antisickling effect of a novel class of five-membered heterocyclic aldehydic compounds, *J. Med. Chem. 47*, 4665−4676.
40. O'Donnell, S., Mandaro, R., Schuster, T. M., and Arnone, A. (1979) X-ray diffraction and solution studies of specifically carbamylated human hemoglobin A. Evidence for the location of a proton- and oxygen-linked chloride binding site at valine 1α, *J. Biol. Chem. 254*, 12204−12208.
41. Perutz, M. F., Kilmartin, J. V., Nishikura, K., Fogg, J. H., Butler, P. J., and Rollema, H. S. (1980) Identification of residues contributing to the Bohr effect of human haemoglobin, *J. Mol. Biol. 138*, 649−668.
42. Fronticelli, C., Pechick, I., Brinigar, W., Kowalczyk, J., and Gilliland, G. (1994) Chloride Ion independence of the Bohr Effect in a Mutant Human Hemoglobin β(V1M+H2deleted), *J. Biol. Chem. 269*, 23965−23969.
43. Fronticelli, C., Sanna, M. T., Perez-Alvaredo, G. C., Karavitis, M., Lu, A.-L., and Brinigar, W. S. (1995) Allosteric Modulation by Tertiary Structure in Mammalian Hemoglobins, *J. Biol. Chem. 270*, 30588−30592.
44. Perutz, M. F., Fermi, G., Poyart, C., Pagnier, J., and Kister, J. (1993) A novel allosteric mechanism in haemoglobin. Structure of bovine deoxyhaemoglobin, absence of specific chloride-binding sites and origin of the chloride-linked Bohr effect in bovine and human haemoglobin, *J. Mol. Biol. 233*, 536−345.
45. Perutz, M. F., Shih, D. T., and Williamson, D. (1994) The chloride effect in human haemoglobin. A new kind of allosteric mechanism, *J. Mol. Biol. 239*, 555−560.
46. Kavanaugh, J. S., Rogers, P. H., Case, D. A., and Arnone, A. (1992) High-resolution X-ray study of deoxyhemoglobin Rothschild 37β Trp→Arg: A mutation that creates an intersubunit chloride-binding site, *Biochemistry 31*, 4111−4121.
47. Sawicki, C. A., and Gibson, Q. H. (1976) Quaternary conformational changes in human hemoglobin studied by laser photolysis of carboxyhemoglobin, *J. Biol. Chem. 251*, 1533−1542.
48. Lukin, J. A., Kontaxis, G., Simplaceanu, V., Yuan, Y., Bax, A., and Ho, C. (2003) Quaternary structure of hemoglobin in solution, *Proc. Natl. Acad. Sci. U.S.A. 100*, 517−520.
49. Turner, G. J., Galacteros, F., Doyle, M. L., Hedlund, B., Pettigrew, D. W., Turner, B. W., Smith, F. R., Moo-Penn, W., Rucknagel, D. L., and Ackers, G. K. (1992) Mutagenic dissection of hemoglobin cooperativity: Effects of amino acid alteration on subunit assembly of oxy and deoxy tetramers, *Proteins 14*, 333−350.
50. Bucci, E., Razynska, A., Kwansa, H., Gryczynski, Z., Collins, J. H., and Fronticelli, C. (1996) Positive and Negative Cooperativities at Subsequent Steps of Oxygenation Regulate the Allosteric Behavior of Multistate Sebacylhemoglobin, *Biochemistry 35*, 3418−3425.
51. Bucci, E., Fronticelli, C., and Gryczynski, Z. (1991) Discontinuous release of heat at successive steps of oxygenation in human and bovine hemoglobin at pH 9.0, *Biochemistry 30*, 3195−3199.
52. Perrella, M., Benazzi, L., Shea, M. A., and Ackers, G. K. (1990) Subunit hybridization studies of partially ligated cyanomethemoglobins using a cryogenic method. Evidence for three allosteric states, *Biophys. Chem. 35*, 97−103.
53. Jayaraman, V., and Spiro, T. G. (1995) Structure of a third cooperativity state of hemoglobin: Ultraviolet resonance Raman spectroscopy of cyanomethemoglobin ligation microstates, *Biochemistry 34*, 4511−4515.
54. Endrizzi, J. A., Beernink, P. T., Alber, T., and Schachman, H. K. (2000) Binding of bisubstrate analog promotes large structural changes in the unregulated catalytic trimer of aspartate transcarbamoylase: Implications for allosteric regulation induced cell migration, *Proc. Natl. Acad. Sci. U.S.A. 97*, 5077−5082.
55. Huang, D. B., Ainsworth, C. F., Stevens, F. J., and Schiffer, M. (1996) Three quaternary structures for a single protein, *Proc. Natl. Acad. Sci. U.S.A. 93*, 7017−7021.

BI050412Q